KECK Geology Consortium
Learning Science Through Research
Published by the Keck Geology Consortium
Short Contributions
Keck Geology Consortium
Volume 33
May 2020
doi: 10.18277/AKRSG.2020.33.16

FLOW BANDS AND MICROLITE TEXTURES IN OBSIDIAN, MINYON FALLS RHYOLITE, AUSTRALIA

ZENJA SEITZINGER, SUNY Geneseo
Research Advisor: Dori Farthing

INTRODUCTION

The Minyon Falls Rhyolite is a Miocene aged, 1.25 km^3 lava dome that was emplaced effusively during the late stages of volcanism of the basaltic Tweed shield volcano in eastern Australia (Smith and Houston, 1995). Extensive weathering and erosion have cut vertically through the lava dome, offering a unique exposure of the crystalline interior and glassy base of the rhyolite (Smith, 1996). Flow bands within the basal obsidian preserve structures and textures indicating accommodation of large shear strains during emplacement of the dome (Smith, 1966; Brown, 2010; Cook, 2011). This study aims to better understand the conduit processes and ascent history of magma that fed the Minyon Falls Rhyolite through a quantitative micro-textural investigation of individual flow bands from the basal shear zone.

Banding in the basal obsidian of the Minyon Falls Rhyolite is well-defined by variations in glass color and microlite concentrations (Fig. 1). Microlites are rod-shaped acicular crystals with lengths typically less than 50 microns that are found ubiquitously in obsidian lavas and pyroclastic obsidian (Ross, 1962). Volatile exsolution in ascending magma causes the liquidus temperatures to increase, creating large effective undercoolings that drive the nucleation and growth of microlites (Hammer and Rutherford, 2002). The study of the number density and size distributions of microlites can therefore provide insight into the dynamics and history of magma ascent in shallow conduits that ultimately feed eruptions of silicic magma (Cashman, 1988; Marsh, 1988; 1998; Castro et al., 2002; Toramaru et al., 2008; Befus et al., 2014).

METHODS

Obsidian samples were collected from the basal shear zone of the Minyon Falls Rhyolite at two localities. The first site is roughly 500 m N-NE of the inferred vent, hereafter referred to as the near vent site and denoted by sample numbers beginning with MR11. Sample MR11.2 was collected near the top of a 0.3 to 0.5-m thick basal breccia overlain by 2.5 m of flow-banded obsidian lava. Samples MR11.6 and MR11.7 were collected within the flow-banded obsidian at approximately 0.1 m and 1 m, respectively, from the contact with the basal breccia. The second site is

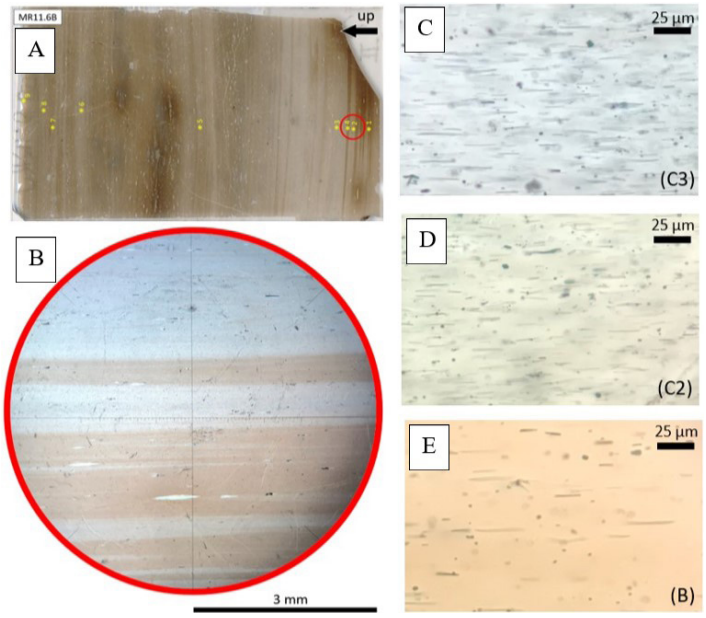

Figure 1. Flow banded obsidian from the Minyon Falls Rhyolite basal shear zone. (A) MR11.6T thin section; yellow stars indicate location of microlite collection sites red circle indicates location of B; up direction is indicated by arrow. (B) Flow banding in plain polarized light (ppl) (4x); (C) C3 band in ppl (40x); (D) C2 band in ppl (40x); (E) B band in ppl (40x).

located at the southern margin of the lava dome about 4 km from the inferred vent. Sample MR02 was collected within the basal breccia at the flow front, which contains deformed clasts elongated roughly parallel to the foliation of the overlying flow-banded obsidian. Microlites at both locations are primarily clinopyroxene (as determined by EDS analysis on the JEOL JSM-6010LA scanning electron microscope at Trinity University) and are generally aligned parallel to banding, except in the vicinity of sparse phenocrysts.

Micro-textural measurements were made for five thin sections; MR11 thin sections 2, 6B (bottom), 6T (top), and 7 represent the relative stratigraphic order from bottom to top respectively at the near vent site. A single thin section was analyzed from sample MR02 (section 9) from the flow front location. All thin sections were cut perpendicular to the flow foliation with the "up" direction parallel to the long edge of the slide (Brown, 2010; Cook, 2011). To establish criteria for selection of bands for quantitative petrographic analyses, a central vertical transect was marked on each thin section parallel to the sample's up direction. At a magnification of 20x, glass color, band thickness, and relative microlite content were determined for each band at the points it crossed the transect.

Microlite populations were characterized for four to nine individual bands for each thin section. Thickness and band type were considered when choosing collection sites in order to provide a data set representative of the entire thin section. A total of 3573 pyroxene microlites were measured within 37 separate collection sites (i.e. individual bands). Using the 40x objective on a petrographic microscope, the apparent length of each microlite within the variable sample volumes was measured with the calibrated scale within the ocular; microlite plunge depth was determined by focusing through the transparent glass onto either end of the microlite; and trend angle relative to the plane of banding was measured using the goniometer on the rotating stage (Castro et al., 2002). True length of each microlite was calculated with simple trigonometry using the apparent length and depth (Befus et al., 2014; 2015). Replicate analyses for ten pyroxene microlites of variable size and orientation measured ten separate times in a band of moderate MND yielded a standard deviation for true microlite length of ± 0.37 microns. Size and orientation measurements were taken for roughly 100 microlites in each collection site (i.e., band), with the sample volume scaled appropriately. Collection volumes varied between 3.75 x 10^4 and 9.26 x 105 μm^3. Microlite number densities were then determined for each band by dividing the number of microlites counted by the volume of the thin section imaged for that collection site.

RESULTS

Four band types were identified within the samples (Table 1): B, brown glass with low to moderate microlite concentrations; C1, cloudy, glass unsuitable for microlite data collection; C2, colorless glass with moderate microlite concentrations; and C3, colorless glass with high microlite concentrations. All band types were found in both the banded and brecciated zones. Bands of brown glass make up on average 14 ±10% of the analyzed samples, while bands of colorless glass, including both C2 and C3, make up on average 69 ±7%, and C1 bands make up 17 ±13%. Band thickness ranges from 0.045 mm to 6.5 mm and is independent of color, type, and stratigraphic position.

Pyroxene microlite number densities and sizes were measured for 14 brown (B) bands and 23 colorless (C) bands, of which 8 were C2 type and 15 were C3 type.

Table 1. Summary of all microlite results.

Band Type	B	C2	C3
# bands quantitatively considered	10	7	13
min MND (m^{-3})	1.08E+14	2.96E+14	5.56E+14
max MND (m^{-3})	4.24E+14	6.88E+14	1.67E+15
avg MND (m^{-3})	2.28E+14	5.12E+14	1.06E+15
Standard Deviation	±1.11E+14	±1.59E+14	±3.42E+14
min CSD slope (-L/Gτ)	-0.136	-0.210	-0.286
max CSD slope (-L/Gτ)	-0.077	-0.121	-0.145
avg CSD slope (-L/Gτ)	-0.107	-0.156	-0.193
Standard Deviation	±0.019	±0.037	±0.046
min CSD y-int [ln(n^0)]	3.85	4.31	4.32
max CSD y-int [ln(n^0)]	4.50	5.30	5.76
avg CSD y-int [ln(n^0)]	4.18	4.69	4.96
Standard Deviation	±0.19	±0.37	±0.42
avg microlite length (μm)	13.1	11.0	10.1
Standard Deviation	±1.3	±1.1	±1.0

This distribution of measurements broadly reflects the abundance of band types within the sample set. MND values range from 1.08 x 10^{14} m^{-3} to 1.67 x10^{15} m^{-3} which is approximately an order of magnitude difference. The ranges, averages, and standard deviations of the characteristic microlite populations for each band type are summarized in Table 1.

Crystal Size Distribution (CSD) plots constructed using 5-µm size bins generate log-linear trends with coefficient of determination (R2) values of 0.85 or greater for the majority of flow bands (Fig. 2). I focus my discussion below on these samples.

Although there is important overlap between the band types (Fig. 3), colorless bands have higher average MNDs, smaller average crystal lengths, steeper characteristic CSD slopes, and higher nucleation densities (derived from CSD intercepts) compared to brown bands (Table 1). When slope of CSDs for individual bands are plotted as a function of MND, a positive correlation is observed, and when CSD slope is plotted as a function of average microlite length, a negative correlation is observed (Fig. 3).

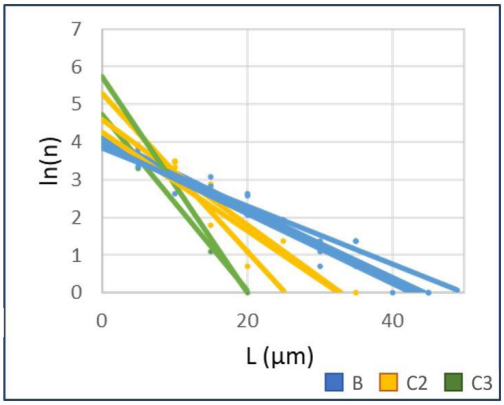

Figure 2. CSD-Fan of MR11.6T bands. Nine separate collection sites are represented here with each trendline color coded to their respective band type.

DISCUSSION

One of the objectives of this study is to assess the timing and location of microlite crystallization and their relation to band formation. Most of the range of microlite size distributions and number densities are observed at the scale of individual thin sections and are not correlated with stratigraphic height or with the degree of microlite alignment within the basal shear zone. These observations indicate that the majority

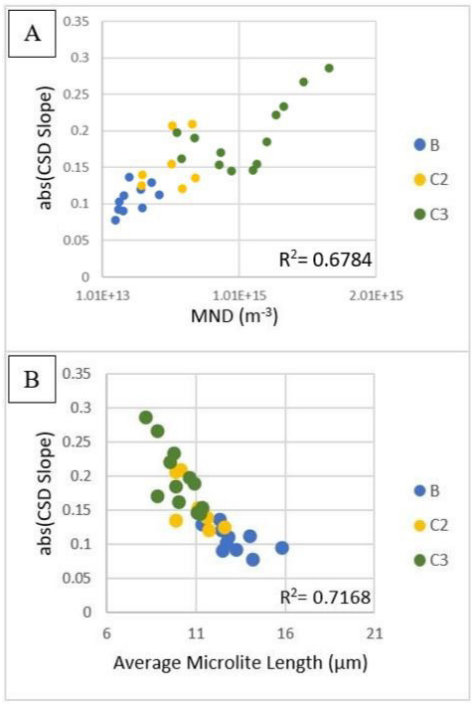

Figure 3. CSD-Fan of MR11.6T bands. Nine separate collection sites are represented here with each trendline color coded to their respective band type.

of acicular pyroxene microlites crystallized during magma ascent in the conduit and do not appear to have been significantly modified by further nucleation or growth during emplacement at the surface. Given that the bands are defined in part by microlite concentrations and sizes, it is reasonable to conclude that the flow bands also formed in the conduit.

Micro-textural variability observed in flow-banded obsidian have been interpreted to reflect variations in ascent rate and residence time during magma transport in shallow volcanic conduits (Castro and Mercer, 2004). Whether high MND values correlates with fast or slow ascent may depend on magma composition. In general, volatile exsolution resulting from magma ascent induces a state of supersaturation ideal for microlite crystallization. A couple between degassing and crystallization may be appropriate for some andesite and dacitic magmas where MND appears to scale with magma ascent rate (Tormamaru et al., 2008). However, in rhyolitic magmas, the loss of volatiles may increase melt viscosity to a point where nucleation and growth of microlites are inhibited (Cassidy et al., 2018). In this scenario, microlites do not reflect the extent, or at least the rate, of degassing as they are kinetically prevented from doing so.

Castro and Mercer (2004) note that MND values for extensively degassed obsidian lavas have a wide range of MND, a range comparable to that reported here for the Minyon Falls Rhyolite. On the basis of kinetic consideration, they propose a model in which microlite variations are governed by the geometry of flow in the conduit. Magma ascent velocity is expected to decrease away from the center of the conduit because the conduit margins exert destructive frictional forces on the ascending melt (Fig. 4). Slow ascent closer to conduit walls allows more time for microlites to crystallize (i.e. higher MND), while faster ascent towards the center of the conduit limits the time for microlites to crystallize (i.e. low MND). However, if CSD slope is a function of growth time (Marsh, 1998), the positive correlation between CSD slope and MND observed here (Fig. 3) is inconsistent with a model based on kinetic limitations to crystallization in highly viscous rhyolitic magma. If so, flow bands with higher MND may in fact reflect faster ascent than bands with lower MND, similar to that proposed for some intermediate magmas.

Alternatively, flow bands may form through a process of repeated shear-related fragmentation and annealing of fragments during magma ascent in in shallow volcanic conduits (Gonnermann and Manga, 2003; 2005; Castro et al., 2005; Tuffen et al., 2003). An ascending melt that experiences excessive shear stress may cross a kinetic boundary shifting from fluid-like to solid-like behavior and fragment into clasts and ash; this process is known as shear-induced fragmentation. Textural heterogeneity, for example expressed as flow banding, may be achieved by repeated fragmentation events followed by melt relaxation and reorganization of internal structure (RFH). At the start of an RFH cycle, the brittle response to the excessive shear stress creates a fracture, resulting in a temporary zone of local decompression (Fig. 4). The localized zone of low pressure surrounding the fracture is expected to initiate volatile exsolution (Castro et al., 2005; Cabrera et al., 2011) and a high degree of undercooling, facilitating the abundant nucleation of microlites (Fig. 4). Bands with high MNDs, smaller average microlite lengths, and steeper CSD slopes (Fig. 3) may therefore be interpreted to have experienced greater degrees of undercooling, while bands with low MNDs, larger average microlite lengths, and shallower CSD slopes

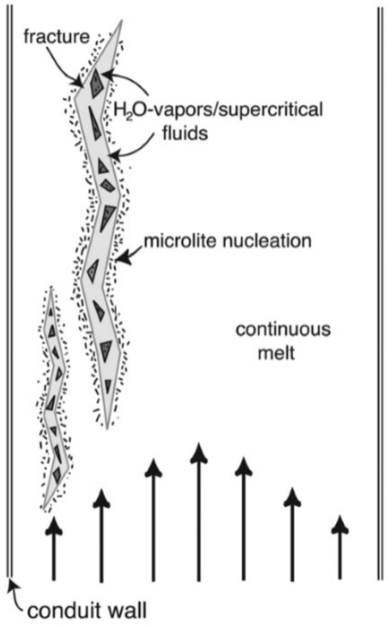

Figure 4. Schematic conduit cross section illustrating possible conduit processes during the ascent and eruption of silicic magma, including flow velocity profile (arrows) and shear-induced fragmentation (Castro et al., 2005).

may have experienced lesser degrees of undercooling.

Analysis of water content profiles transecting healed faults in pyroclastic obsidian revealed low water content along structures interpreted as fault suture zones and both abrupt and gradual increases in water content moving further away (Cabrera et al., 2011). These results raise the possibility that local zones within the ascending magma may experience individualized degassing histories in response to melt fracturing. If correct, the Minyon Falls microlite characteristics (Fig. 3), including the fan-like pattern of CSD trendlines within a single thin section (Fig. 2) may be interpreted to record variation in water exsolution and associated undercooling within proximity to shear-induced fractures (Fig. 4). The greatest MND and steepest CSD slopes may record zones of greater volatile exsolution closest to the fracture; the decrease in MND and CSD slope steepness may result from increasing distance away from the fracture.

Alternatively, the degassing and undercooling driving the microlite crystallization preserved in any flow band may be dependent on the depth of shear fragmentation. Melt fracturing at deeper levels in the conduit should induce lesser extents of degassing and smaller undercooling compared to fragmentation

at shallower levels. If crystallization is in response to the sudden gas loss from the melt, lower effective undercooling at greater depth may then lead to lower MND and shallower CSD slopes. Continued ascent and fragmentation at shallower levels would lead to bands with higher MND and steeper CSD slopes.

In either case, as shear stresses relax following fragmentation, the melt reverts to fluid-like behavior and anneals the space created by the opened fracture (Tuffen et al. 2003). The brecciated magma surrounded by a microlite rich zone may deform plastically and elongate by the ascending forces. Repeated fragmentation events may create intermittent fracture networks that promote the permeable flow of exsolved volatiles to travel through and escape, resulting in an open system degassing mechanism that is consistent with effusive eruptions (Cabrera et al., 2011).

CONCLUSIONS

Based upon the microanalysis of flow bands within the basal shear zone of the Minyon Falls lava dome, the following conclusions can be made:

(1) The lack of any correlation between band thickness, glass color, MND, and microlite size and preferred orientation with stratigraphic height within the basal shear zone suggests that microlite-defined flow bands form during magma ascent.

(2) Colorless bands are characterized by high MNDs, smaller average microlite lengths, and steeper CSD slopes, while brown bands are characterized by low MNDs, larger average microlite lengths, and shallower CSD slopes.

(3) Given that number densities and size distributions of microlites vary widely on the scale of a thin section, individual flow bands are interpreted to provide a record of spatially complex variations in water exsolution rate and degree of undercooling during transport. The observed textural variations may be explained by variable ascent rate and/or repeated fragmentation and healing events (RFH) within the shallow volcanic conduit.

ACKNOWLEDGEMENTS

This material is based upon work supported by the Keck Geology Consortium and the National Science Foundation under Grant No. 1659322.

REFERENCES

Befus, K.S., Manga, M., Gardner, J.E., and Williams, M., 2015, Ascent and emplacement dynamics of obsidian lavas inferred from microlite textures: Bulletin of Volcanology, v. 77, p. 1-17, doi: 10.1007/s00445-015-0971-6.

Befus, K.S, Zinke, R.W., Jordan, J.S., Manga, M., and Gardner, J.E., 2014, Pre-eruptive storage conditions and eruption dynamics of a small rhyolite dome: Douglas Knob, Yellowstone volcanic field, USA: Bulletin of Volcanology, v. 76, p. 1-12, doi: 10.1007/s00445-014-0808-8.

Brown, A., 2010, Flow dynamics, strain history and structural evolution of the basal shear zone of silicic lava, Minyon Falls Rhyolite, New South Wales, Australia. Unpublished Honors Thesis, University of Queensland, p. 53.

Cabrera A., Weinberg, R.F., Wright, H.M.N., Zlotnik, S., and Cas, R.A.F., 2011, Melt fracturing and healing: a mechanism for degassing and origin of silicic obsidian: Geology, v. 39, p. 67-70, doi: 10.1130/G31355.1.

Cashman, K.V., 1988, Crystallization of Mount St. Helens 1980-1986 dacite: A quantitative textural approach: Bulletin of Volcanology, v. 50, p. 194-209.

Cassidy, M., Manga, M., Cashman, K., and Bachmann, O., 2018, Controls on explosive-effusive volcanic eruption styles: Nature Communications, doi: 10.1038/s41467-018-05293-3.

Castro, J.M., Dingwell, D.B., Nichols, A.R.L., and Gardner, J.E., 2005, New insights on the origin of flow bands in obsidian: Geological Society of America Special Paper 396, p. 55-65, doi: 10.1130/2005.2396(05).

Castro, J.M. and Mercer, C., 2004, Microlite textures and volatile contents of obsidian from the Inyo volcanic chain, California: Geophysical Research Letters, v. 3, doi:10.1029/2004GL020489.

Castro, J., Manga, M., and Cashman, K., 2002,

Dynamics of obsidian flows inferred from microstructures: insights from microlite preferred orientations: Earth and Planetary Science Letters, v. 199, p. 211-226, doi: 10.1016/S0012-821X(02)00559-9.

Cook, S., 2011, Ascent and emplacement history of silicic lava inferred from microlite and bubble shapes and orientations Minyon Falls Rhyolite, New South Wales, Australia, Unpublished Honors Thesis, University of Queensland, p. 250.

Gonnermann, H.M., and Manga, M., 2003, Explosive volcanism may not be an inevitable consequence of magma fragmentation: Nature, v. 426, p. 432-435.

Gonnermann, H.M., and Manga, M., 2005, Flow banding in obsidian: A record of evolving textural heterogeneity during magma deformation: Earth and Planetary Science Letters, v. 236, p. 135-147, doi: 10.1016/j.epsl.2005.04.031.

Hammer, J.E. and Rutherford, M.J., 2002, An experimental study of the kinetics of decompression-induced crystallization in silicic melt: Journal of Geophysical Research, v. 107, doi: 10.1029/2001JB000281.

Marsh, B.D., 1988, Crystal Size Distribution (CSD) in rocks and the kinetics and dynamics of crystallization: Contributions to Mineralogy and Petrology, v. 99, p. 277-291.

Marsh, B.D., 1998, On the interpretation of crystal size distributions in magmatic systems: Journal of Petrology, v. 39, p. 553-599.

Ross, C.S., 1962, Microlites in glassy volcanic rocks: American Mineralogist, v. 47, p. 723-740.

Smith, J.V., 1996, Ductile-brittle transition structures in the basal shear zone of a rhyolite lava flow, eastern Australia: Journal of Volcanology and Geothermal Research, v. 72, p. 217-223, doi: 10.1016/0377-0273(96)00009-1.

Smith, J.V., and Houston, E.C., 1995, Structure of lava flows of the Nimbin Rhyolite, northeast New South Wales, Australian Journal of Earth Sciences, v. 42, p. 69-74.

Toramaru, A., Noguchi, S., Oyoshihara, S., and Tsune, A., 2008, MND (microlite number density) water exsolution rate meter: Journal of Volcanology and Geothermal Research, v. 175, p. 156-167, doi: 10.1016/j.jvolgeores.2008.03.035.

Tuffen, H., Dingwell, D.B., and Pinkerton, H., 2003, Repeated fracture and healing of silicic magma generate flow banding and earthquakes: Geology, v. 31, p. 1089-1092.